Edge pedestal physics and its implications for ITER

Y.Kamada[1], A.W.Leonard[2], G.Bateman[3], M.Becoulet[4], C.S.Chang[5], T.Eich[6], T.E.Evans[2], R.J.Groebner[2], P.N.Guzdar[7], L.D.Horton[6], A.Hubbard[8], J.W. Hughes[8], K.Ida[9], G.Janeschitz[10], K.Kamiya[1], A.Kirk[11], A.H.Kritz[3], A.Loarte[12], J.S.Lonnroth[11], C.F.Maggi[6], R.Maingi[13], H.Meyer[11], V.Mukhovatov[14], T.Onjun[15], M.Osipenko[16], T.H.Osborne[2], N.Oyama[1], G.W.Pacher[17], H.D.Pacher[18], A.Y.Pankin[3], V.Parail[11], A.R.Polevoi[14], T.Rognlien[19], G.Saibene[12], R.Sartori[12], M.Shimada[14], P.B.Snyder[2], M.Sugihara[14], W.Suttrop[6], H.Urano[1], M.R.Wade[2], H.R.Wilson[20], X.Q.Xu[19], M.Yoshida[1], and the ITPA Edge & Pedestal Physics Topical Group

[1] Japan Atomic Energy Agency, [2] General Atomics, [3] Lehigh Univ., [4] Association Euratom-CEA, [5] New York Univ., [6] Association Euratom-IPP, [7] Univ. Maryland, [8] MIT Science and Fusion Center, [9] NIFS, [10] FZK-PL-Fusion, [11] Association Euratom-UKAEA, [12] EFDA-CSU, [13] Oak Ridge National Laboratory, [14] ITER International Team, [15] Thammasart Univ., [16] Kurchatov Institute, [17] Hydro-Quebec, [18] INRS, [19] Lawrence Livermore National Laboratory, [20] Univ. of York,   e-mail of the first author: kamada.yutaka@jaea.go.jp

Abstract. This paper summarizes recent progress of the H-mode pedestal physics and its implication for ITER achieved in the world pedestal research community. The complex parameter linkages determining the pedestal structure and its dynamics have been identified. The pedestal width is determined by both plasma and neutral transport. The trigger of the type-I ELM has been explained successfully by the peeling-ballooning modes. The improved pedestal diagnostics revealed the evolution of the type I ELM cycle (crash and recovery). The measurements of the ELM crash show poloidal asymmetry of erosion inside the separatrix and helical filament structure expanding into the SOL. This nonlinear explosive evolution of the filaments has been predicted theoretically and reproduced numerically. A variety of small and no-ELM regimes have been reproduced in multiple devices by matching the non-dimensional parameters and the plasma shape, and accessibility to these regimes has been identified and categorized. In both type I and small/no ELM regimes, plasma rotation plays important roles in determining the pedestal width and ELM size and frequency. The modeling capability integrating the core, pedestal and SOL regions has also achieved remarkable progress. Based on these results, the pedestal height required for ITER has been evaluated, the ELMing ITER base line scenario has been simulated, type I ELM mitigation methods have been evaluated for ITER.

1. Introduction

The standard and advanced ITER operation modes are envisaged to be based on the H-mode. The H-mode pedestal sets the boundary conditions for the core, SOL and divertor plasmas, and it plays a central role in achieving the desired integrated plasma performance. In particular, predicted fusion gain Q in ITER depends strongly on the pedestal temperature at the operational density. At the same time, the ELM heat load on to the divertor plates should be maintained at a tolerable level. The H-mode pedestal is a complex system determined by both plasma processes and atomic processes in a narrow layer. The pedestal evolves with multiple time scales from the growth time of ideal MHD instabilities to the wall saturation time of particles. The goals of pedestal research are to understand this complex system in order to improve predictive capability for ITER, and to develop control schemes for the pedestal parameters and ELMs. The critical issues [1] for achieving these goals are 1) identification of the processes determining the pedestal structure, 2) understanding and evaluation of the type I ELM trigger and energy losses, 3) development and evaluation of small / no ELM regimes, 4)type I ELM mitigation techniques, and 5) construction of integrated prediction codes. For all of these issues, remarkable progress has been achieved recently by integrating the results obtained in single- and inter-machine experiments (Alcator C-Mod, ASDEX-U, DIII-D, JET, JFT-2M, JT-60U, MAST and NSTX) with theoretical progress.

2. Identification of the processes determining the pedestal structure

2-1) Parameter linkage determining the pedestal structure

The H-mode pedestal is characterized by the steep gradient of density, temperature and thus pressure in a narrow width Δ_{ped} (Fig.1(a)). The large pressure gradient induces the edge bootstrap current and produces the radial electric field. The pedestal width Δ_{ped} seems to be determined by transport and the pressure gradient is limited by MHD instabilities (ELMs). Figure 1(b) shows parameter linkages determining the pedestal structure and evolution revealed by world pedestal researches. The pedestal stability limit (ELMs) is determined by a combination of the pressure gradient, the edge bootstrap current, plasma shape, the plasma rotation and the Shafranov shift. The produced edge flow shear and magnetic shear suppress turbulence and determine the pedestal width.
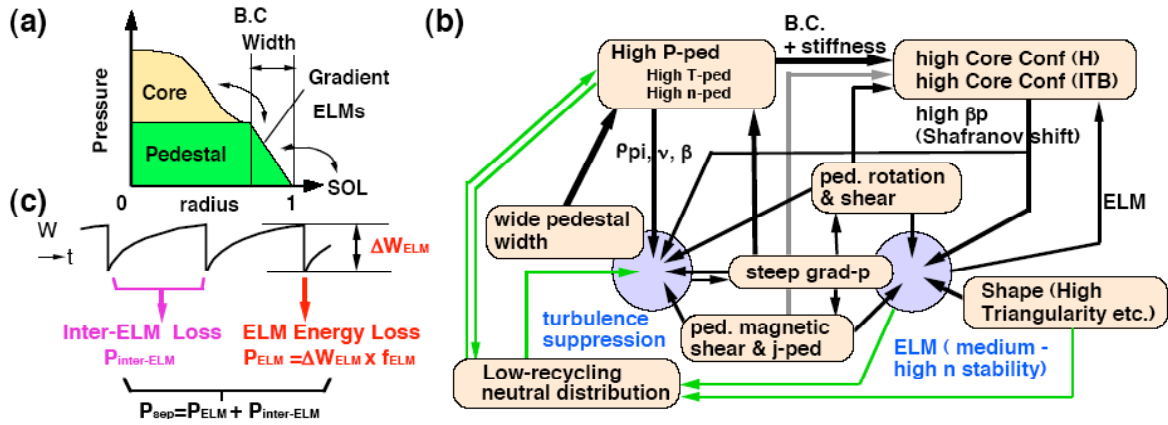
Fig.1: (a) Schematic radial profile of plasma pressure, (b) Parameter linkages determining the pedestal structure and dynamics. (c) Stored energy evolution of the ELM cycle.

Penetration of neutrals also seems to affect the density pedestal width. A steep pressure gradient and wide Δ_{ped} enhances the pedestal pressure. The high pedestal pressure allows a high pedestal temperature at a given pedestal density. High pedestal temperature improves the core confinement (depending upon profile stiffness). And then, if the core confinement (or β_p) is improved, the pedestal stability is improved. Figure 1(c) shows a sketch of stored energy evolution across ELMs. The important challenge for us is to understand the dynamics of the pedestal system at the ELM crash and in the inter-ELM phase.

2-2) Pedestal height required for ITER

Prediction of the fusion gain Q in ITER by transport modeling depends strongly on the prediction of the temperature at the top of the pedestal T_{ped}. Simulations using various core transport models in combination with various models for the pedestal illustrate the sensitivity of ITER performance to uncertainties in the projected pedestal characteristics. Figure 2 shows the resulting Q as a function of T_{ped} at the operational density for the MMM95, GLF23 and Weiland models [2]. Along the horizontal axis, the pedestal ranges from several pedestal models are indicated. Although some theory based empirical models predict a T_{ped} ~4keV with Q>10 in ITER, the range of predicted T_{ped} by various pedestal width models is still significantly wide. The critical edge pressure gradient in ITER has been evaluated based on the peeling-ballooning model (Fig.3), which shows the limit of T_{ped} increases nearly proportional to D_{ped}/a, and T-ped~5keV at D_{ped}/a =0.03 ($n_{-ped}=7x10^{19}m^{-3}$) [3].
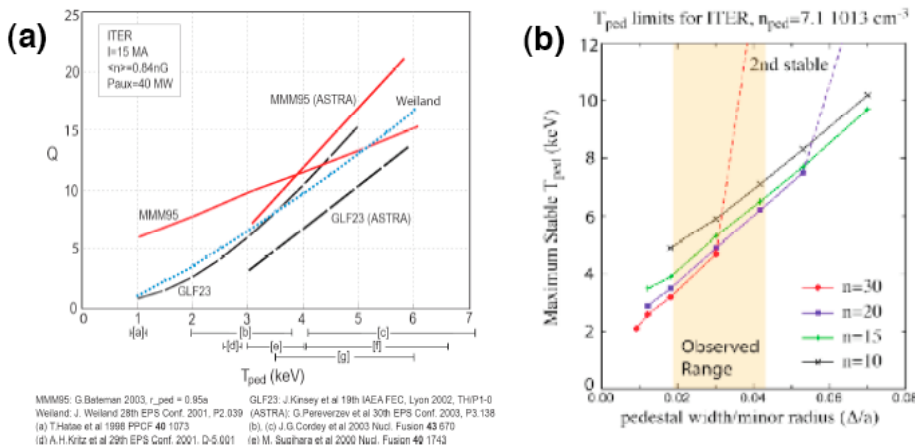

Fig.2: (a) The fusion gain Q in ITER as a function of the pedestal temperature predicted by transport models and pedestal temperature models[2].
(b)Predictions of the maximum stable pedestal temperature for ITER as a function of pedestal width from the ideal stability calculations for a range of density [3].

2-3) Pedestal width and pedestal stored energy

The edge transport barrier recovers quickly after the type I ELM crash. JT-60U reported that, between ELMs, the energy transport decreases with decreasing ν* (Fig.3) and the value is close to the ion neoclassical level [4]. ASDEX-U reported that the ion transport in the edge transport barrier ETB does not seem to be at the neo-classical level, suggests that residual turbulence still control the transport through the ETB [5]. Although the transport does not reach the pure neoclassical level, it seems that the pedestal width is determined by significant reduction of turbulence. The multi-machine comparison experiments [6,7] have suggested that the pedestal temperature width is

determined by the magnetic field structure and non-dimensional parameters determining the plasma process. Figure 4 shows electron density and temperature profiles in DIII-D and JET with matched profiles of β, ν_e^* and ρ^* [6]. Electron temperature profiles (Fig.4(b)) and hyperbolic tangent fits (curves) neither show significant difference in temperature barrier width between JET (black stars) and DIII-D (red squares), nor for a variation of ρ^* in DIII-D (red squares versus green crosses).

For the pedestal density profile, a dimensional parameter, neutral penetration depth, also plays a role. Figure 4(a) shows that in DIII-D and JET, a neutral penetration model (curves) explains the density profiles [6]. On the other hand, no evidence has been found that the ETB width in ASDEX-U [5] scales with the neutral penetration depth into the core plasma, and suggested that the detailed shape of the edge density profile is due to a combination of source and transport effects. This may be the reason why the dependence of density pedestal width is different in different conditions and in different devices. Also in C-Mod, the density pedestal width does not change with changing the pedestal density. In C-Mod, edge neutral transport is studied using one-dimensional kinetic modeling. In both experiment and modeling, the C-mod density pedestal exhibits a weakly increasing pedestal density and a nearly invariant density pedestal width as the D^0 source rate increases [8].

Another key parameter determining the pedestal structure was uncovered by the JET & JT-60U comparison experiment [9] with matched 'absolute' global parameters showing that the pedestal pressure is higher in JET (Fig.5(a)). One possible reason for this difference is the magnitude of the toroidal field ripple. Ferritic steel tile installation in JT-60U for reduction of the toroidal

Fig.3: Inter-ELM confinement in JT-60U as a function of the edge collisionality: tE*decreases with collisionality as $\nu^{*\xi}$, $\xi=-0.6$ [4].

Fig.4: Electron density and temperature profiles in DIII-D and JET with matched profiles of β, ν_e^* and ρ^* [6].

magnetic field ripple has revealed that the ripple loss of fast ions and the resulting shift of toroidal plasma rotation V_T into co-direction increase the pedestal height (Fig.5(b)) [10]. In addition, the inter-ELM transport loss is reduced. Moreover, p_{ped} is raised even at a given V_T, suggesting that the reduction of TF ripple itself also plays a role in increasing p_{ped} (Fig.5(b)). For increased p_{ped} due to enhanced V_T in the co-direction and the reduction of TF ripple, the pedestal width became wider. Related to these observations, an additional thermal ion transport enhanced by the field ripple has been proposed [11].

The pedestal structure in advanced operation modes is within the parameter dependence of the standard H-mode, and the pedestal stored energy tends to increase with increasing the core stored
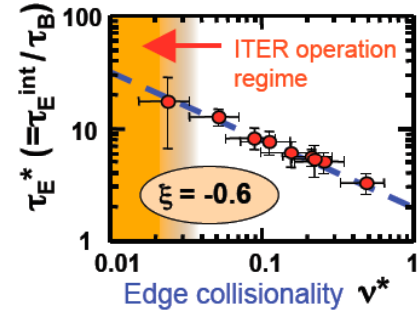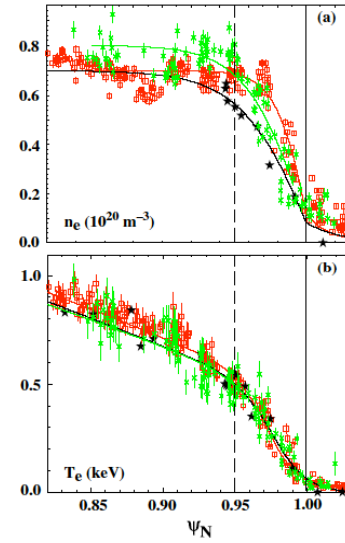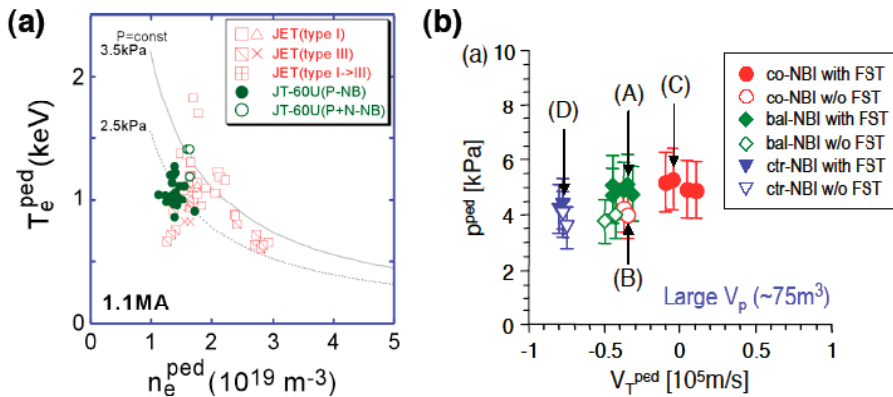

Fig. 5: (a) Pedestal temparature vs. density in JET / JT-60U experiment with matched 'absolute' global parameters [9]. (b) Dependence of pedestal pressure pped on toroidal rotation VTped in theJT-60U type-I ELMy H-mode plasma, where open symbols correspond to without ferritic steel tilse (FST).
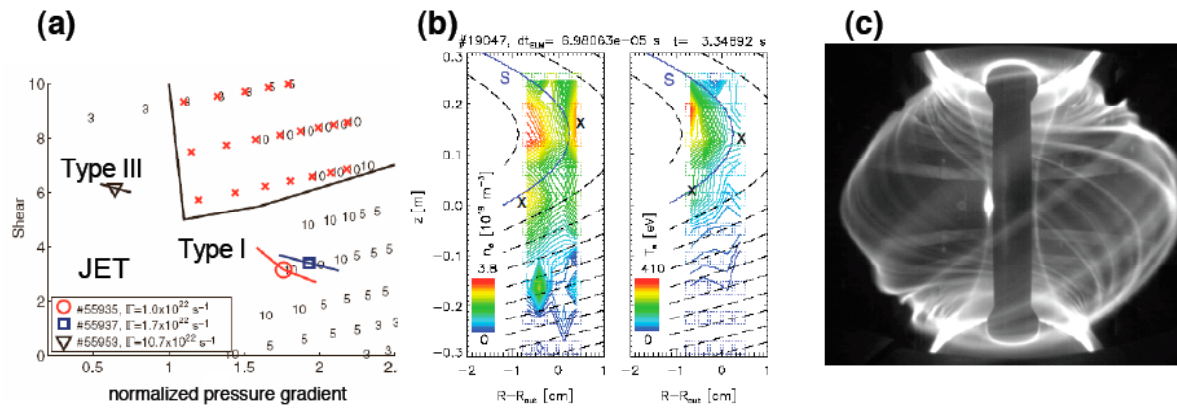
Fig.6: (a) Pedestal stability of type I H-mode in JET determined by high n peeling-ballooning mode [15]. (b) Two-dimensional profiles of electron density (left) and electron temperature (right) in ASDEX-U[5] by firing five Nd–YAG lasers in a burst of total duration 2μs, centred at the peak of the ELM Dα emission. (c) High-speed video image of the MAST plasma obtained at an ELM [17]

The pedestal structure in advanced operation modes is within the parameter dependence of the standard H-mode, and the pedestal stored energy tends to increase with increasing the core stored energy or β_p [12-14]. An interpretation is that the increasing total bp increases Shafranov Shift leading to an improvement in pedestal stability [12].

The remaining largest issue is that we still do not have a conclusive prediction of the pedestal width in ITER.

3) Type I ELM trigger, evolution, energy losses and recovery
3-1) Type I ELM trigger and evolution

Tokamak experiments have confirmed that the trigger of type-I ELMs can be explained systematically by the peeling-ballooning modes. Figure 6(a) shows an example of JET [15] where the type I ELMing edge is close to the stability boundary of n=10. Now research on ELM crash dynamics, time scale and spatial structure, has progressed to the nonlinear evolution of the mode. Improved pedestal diagnostics have revealed the 2-3D structure of the ELM crash, such as poloidal asymmetry of erosion inside the separatrix and helical filament structure expanding into the SOL [16]. Figure 6(b) shows two-dimensional profiles of electron density (left) and electron temperature (right) in ASDEX-U [5] . The profiles are obtained by firing five Nd–YAG lasers in a burst of total duration 2μs, centered in this case at the peak of the Dα emission caused by an ELM. Strong local perturbations of both density and temperature are observed in the near SOL (marked by X in the contour plots), consistent with the ELM being a moderate toroidal mode number ($n \approx 8$–20) instability. More striking and beautiful features of the ELM are seen in the filamentary explosion firstly captured in MAST (Fig.6(c) [17]. The filaments exist for the time over which particles are being released into the scrape off layer. They start off at the plasma edge rotating at the velocity of the pedestal, and then decelerate toroidally and accelerate radially outwards. As the filaments propagate radially they remain aligned with the local magnetic field line [18].

3-2) ELM energy loss and recovery

Multi-machine data analyses shows that $\Delta W_{ELM}/W_{ped}$ (energy loss by an ELM / pedestal stored energy) tends to increase with decreasing pedestal collisionality ν^*, and the value is 5- 20% at the expected ν^* in ITER [19]. The mean value is higher than the allowable level of 4-5% in ITER. At a given ν^*, DW_{ELM}/W_{ped} tends to increase with triangularity [20], and with increasing co-directed toroidal rotation [21] (Fig.7(a)). JET has shown that the ν^*-dependence of the efflux is large for conductive loss and small for the convective loss [22] (Fig.7(b)). Such energy release by an ELM is carried partly (<20%) by the filaments mentioned above [16]. The main loss channel has yet to be identified. One possibility is that the filaments tear the closed flux surfaces allowing parallel transport from the pedestal to the divertor. Another possibility is that the structure of the edge Er shear is suddenly broken by the ELM crash (Fig.8(a)) [23]. DIII-D has reported that the eroded area in the core plasma is consistent with the eigen function distribution of the calculated peeling mode.
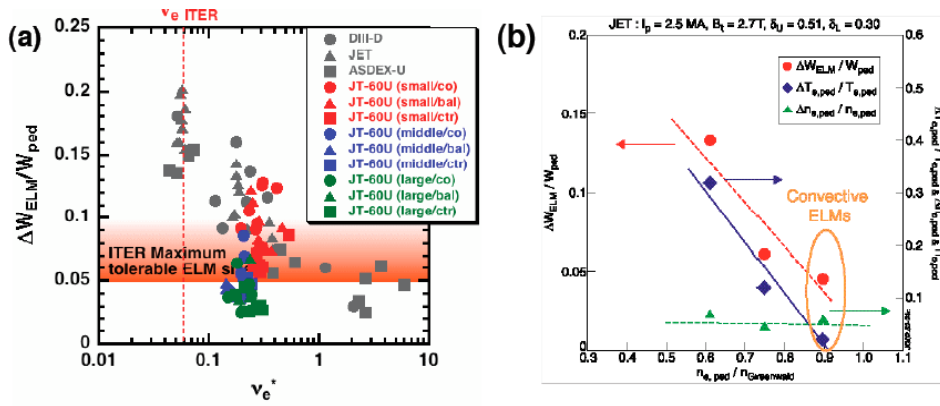
Fig.7: (a) Type I ELM energy loss normalized to the pedestal stored energy ($\Delta W_{ELM}/W_{ped}$) versus collisionality. JT-60U data shows the ELM loss changes with co-, balance- counter- NB injection [21]. (b) $\Delta W_{ELM}/W_{ped}$ and pedestal density and temperature drop versus pedestal density normalized to the Greenwald limit in JET [22].
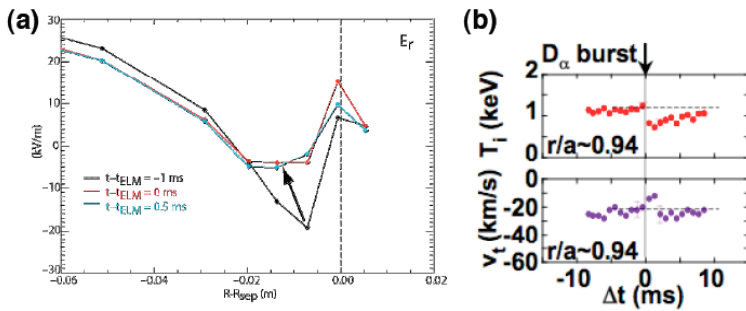

Fig.8: (a) Radial profile od Er measured just before and after an ELM crash in DIII-D [23]. (b) Change in pedestal (r/a=0.94) ion temperature and toroidal rotation across an ELM in JT-60U [24].

DIII-D [23] and JT-60U discharges(Fig.8(b)) [24] reported that, after an ELM crash, recovery of the pedestal rotation profile takes place faster than recovery of the pedestal pressure. Then the edge pressure recovers in the time scale of the inter-ELM transport treated above in Sec.1-3.

3-3) Progress of the Peeling-Ballooning Theory

The success of the peeling-ballooning theory [25] for ELMs is a good example of how the encouragement of collaboration between institutes can bring benefits. The model has been confirmed to a high degree of confidence on a number of tokamaks for the onset of large ELMs. The linear theory can only provide quantitative information about the onset of ELMs. To understand the energy expelled requires a non-linear theory. A non-linear analytic theory, valid early in the evolution of a ballooning mode, predicts that filamentary structures should grow explosively [26]. A number of codes support this general result [27,28]. Figure 9 shows this nonlinear explosive evolution of the filaments reproduced numerically by using the 3D electromagnetic two-fluid code BOUT [28]. It was found that the early behaviour of the modes is similar to expectations from linear, ideal peeling-ballooning mode theory, with the modes growing linearly at a fraction of the Alfven frequency. In the non-linear phase, the modes grow explosively, forming a number of extended filaments which propagate rapidly from the outer closed flux region into the open flux region towards the wall.

It remains for us to understand the mechanisms responsible for smaller ELM regimes [25,29]. One key is the change of surface current across an ELM, which should be evaluatedexperimentally.
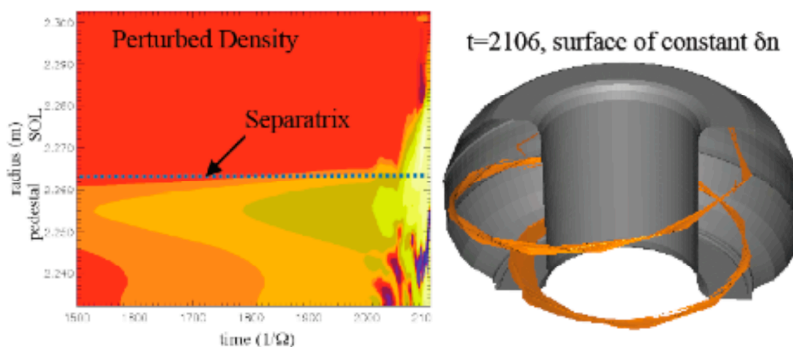

Fig.9: (a) Contour plot of the evolutions of the perturbed density on the outboard midplane. (b) 3D structure of thesurface of constant perturbed density at the explosive burst (t=2106). simulated by BOUT [28]

Or perhaps the answer lies in the non-linear mechanisms. A final twist to the tale is that recent analytic theory finds that sufficient edge current density is required to cause the filaments to be ejected outwards towards the wall (otherwise they erupt inwards, towards the plasma core) [30]. One can postulate that if the filaments erupt into the core plasma, this would give rise to smaller ELMs than if they explode outwards.

4) Development of small / no ELM regimes

Small/no ELM regimes such as EDA, Grassy ELM, HRS, QHmode,type II and V ELMs with good confinement properties have been obtainedin Alcator C-Mod, ASDEX-Upgrade, DIII-D, JET, JFT-2M, JT-60U and NSTX. All these regimes show considerable reduction of instantaneous ELM heat load onto divertor target plates in contrast to conventional type I ELMs, and the ELM energy losses are evaluated to be less than 5% of the pedestal stored energy [31]. In addition, almost all of these small/no ELM regimes have been reproduced in multiple devices by matching the

Table 1: Summary of global characteristics in various small/no ELM regimes. RL in column $\Delta W_{ELM}/W_{ped}$ means that values in the column show maximum value evaluated from the resolution limit of the diagnostics.[31]

Type (Device)	ELM size ($\Delta W_{ELM}/W_{ped}$)	edge fluctuaions	collisionality	confinement property	operational conditions
Type II (AUG)	$<2\pm1\%$(RL)	BB	$1.3<\nu_e^*<3.4$	$H_{89PL} \leq 2$ $H_{98,y2} \leq 1$	$0.85<\bar{n}_e/n_{GW}<0.95$ $q_{95} >3.5-4$ QDN($\delta \sim 0.4$)
(JET)	$<4-5\%$(RL)	BB	$0.8<\nu_e^*<1.2$	$H_{98,y2} \leq 1$	$n_{ped}/n_{GW} \geq 0.7$ $\delta > 0.4$
Grassy (JT-60U)	$<1\%$	none	$0.2<\nu_e^*<0.8$	$H_{89PL} \leq 2.7$ $H_{98,y2} \leq 1$	$\delta \geq 0.4$ $q_{95} \geq 4(at\ \delta\geq0.6)$
(JET)	$<4-5\%$(RL)	none	$1.2<\nu_e^*<1.9$	$H_{98,y2} \sim 1.1$	$\beta_p \geq 1.4$
(AUG)	$<2\pm1\%$(RL)	none	$\nu_e^* \sim 0.8$	$H_{89PL} \leq 1.8$ $H_{98,y2} \leq 1$	
QH (DIII-D)	no ELM	EHO	$0.04<\nu_e^*<0.3$	$H_{89PL} \leq 2.2$	CTR-NBI
(AUG)	no ELM	EHO+HFO	$\nu_e^* \sim 0.3$	$H_{89PL} \leq 1.6$	large gap
(JT-60U)	no ELM	EHO	$0.4<\nu_e^*<0.7$	$H_{89PL} \leq 1.7$	$\bar{n}_e/n_{GW} < 0.47$
(JET)	no ELM	EHO		$H_{98,y2} \sim 1$	$q_{95} \geq 3.3$
EDA (C-Mod)	no ELM	QCM	$\nu_e^* \geq 2$	$H_{89PL} \sim 1.9$	boronization $q_{95}>3.2, \delta>0.35$
HRS (JFT-2M)	no ELM $<0.1\%$(RL)	LF+HF	$\nu_e^* \geq 2$	$H_{89PL} \leq 1.6$	boronization $q_{95}\geq3, \delta>0.35$
Type V (NSTX)	$<4.5\%$(RL)	none	$\nu_e^* \geq 2$	$H_{97L} \sim 2.2$	LSN(lower κ)

non-dimensional parameters and the plasma shape (for example[32-35]). Table I summarizes characteristics of these regimes in terms of the operational space in non-dimensional pedestal parameters and requirement of plasma shape/configuration [31]. Except for Grassy ELMs and type V ELMs [36], the edge fluctuations (such as EHO, QCM) enhance transport, in particular the particle transport, and the pedestal pressure is kept below the type I ELM limit. The Grassy ELMs have a narrow ELM affected area compared to type I ELMs [37]. Figure 10 summarizes the operational area of small/no ELM regimes in ν_e^* -n_{ped}/n_{GW} space; current devices cannot match both parameters at once. Up to now, only the grassy ELM and QH-mode regimes have been achieved at collisionalities close to ITER. The small/no ELM regimes also tend to appear at high triangularity or at quasi double null configurations. Better understandings of the effects of collisionality, plasma
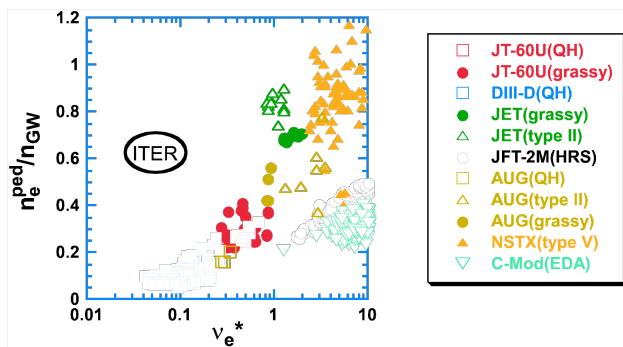

Fig.10: Operational space in ν_e^* versus n_{ped}/n_{GW} for small/no ELM regimes and the type I ELM regime. Different colors show different devices. Open symbols show small/no ELM regimes with edge fluctuations [31].
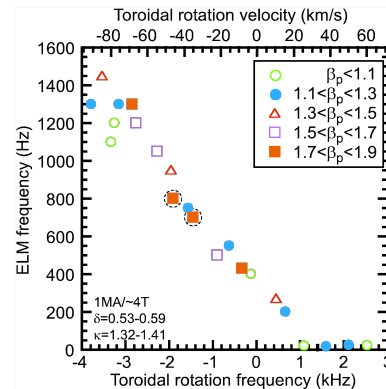
Fig.11: ELM frequency versus toroidal rotation velocity and frequency for Grassy ELMs (Vt<+25km/s) and type I ELMs in JT-60U.Positive sign of the horizontal axis means co- direction [38].

shape and driving mechanisms of the edge fluctuations are needed. In addition, the plasma rotation seems to be an important parameter. The counter rotation produces the QH mode. In addition, by utilizing the co-, counter- and perpendicular NBs, JT-60U demonstrated grassy ELM frequency increases almost linearly up to 1400 Hz with increasing counter (CTR) plasma rotation as shown in Fig.11 [38]. Even in the no-rotating plasma with balanced-NBIs, higher ELM frequency of ~400 Hz has been observed without large ELM energy loss. When the plasma rotation becomes higher than 1 kHz in the co-direction to the plasma current, type I ELMs with a frequency of 20 Hz was observed.

5) type I ELM mitigation and control

Among various mitigation techniques of type-I ELMs, pellet injection is a good candidate for ITER. ASDEX-U demonstrated that type-I ELMs can be triggered by pellet injection when pellet penetration is $(0.5 - 1)$ x Δ_{ped} [39]. With increasing pellet injection frequency, the ELM frequency, f_{ELM}, is completely governed by the pellet frequency and the ELM amplitude is reduced. In the ITER case, the natural f_{ELM} is expected to be ≈ 1.6 Hz with ΔW_{ELM}=20MJ and P_{ELM} (ELM energy loss) $\approx 40\%$ of the average energy loss across the separatrix P_{sep}=80MW. This heat load on the divertor plate is 2-3 times higher than the allowable level. Thus, at least f_{ELM} of 3-5 Hz is required. An ablation calculation with the B2/Eirene code has shown that, for the required penetration depth ($\approx 0.5\Delta_{ped}$), pellet size of $d_{pel}\approx 3.5$ mm is

Fig. 12: Operation window (shown by red asterisks) of HFS pellet injection for ELM control in ITER

necessary when the with 400 m/s [40]. The injection frequency and size must be compatible with fueling and exhaust. Figure 12 shows the operation window (red asterisks) of pellet injection for ELM control in ITER [41]. Depending on the particle confinement time τ_p in the core plasma, pellet size (fueled particle) must be restricted to maintain the particle balance in the core plasma (red solid line). Other constraints are exhaust limit (150 Pam^3/s :black dashed line) and penetration limit ($\approx 0.5\Delta_{ped}$: green dashed line). The expected range of τ_p is depicted by horizontal bar [42]. It is seen from Fig. 12, significant operation window can be reserved and fueling pellet from HFS could be commonly used both for fueling and ELM pace making. One concern is that the confinement degradation may be significant, e.g., 10~15% reduction when f_{ELM} is increased by a factor of 2-3, if confinement degradation scales with $f^{0.16}$ as observed in ASDEX-U [43].

A control scheme utilizing resonant magnetic perturbation (RMP) could be another good candidate. This technique has been developed in DIII-D [44,45], where elimination of ELMs at ITER's collisionality has been demonstrated. As shown in Fig.13, Type I ELMs disappear when external field is applied. The RMP increases transport, particularly particle transport through the pedestal. Physics issues include general scaling to ITER's parameters, compatibility of operation at high density, interaction with pedestal stability limits at higher shaping and penetration of the RMP with plasma rotation. Magnetic perturbation and its effects on the edge ergodization and on the island formation in the core plasma for various ergodic coil systems and for q profiles of three ITER scenarios (reference H-mode, hybrid, ITB) have been studied [46]. For the coil system inside the TF coils but outside the vacuum vessel (VV) around the 18 horizontal ports, the required coil current is ≈ 200 kA. However, the magnetic perturbation generates an increasing island size towards the center of the plasma (e.g., island size is 7-10 cm at q=4/3). It has been found that coil systems installed inside the VV around rows of blanket modules above and below the horizontal port can naturally achieve the required edge ergodization with much less current (≈ 20 kA) and with a decreasing perturbation towards the plasma center (5-7 cm
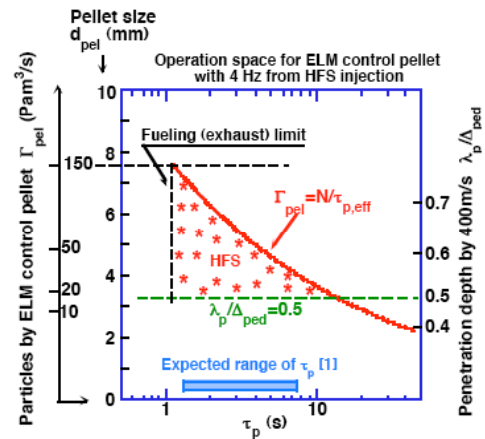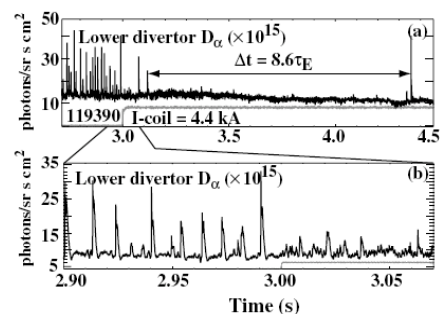

Fig.13: Type I ELMs disappear when external field is applied in DIII-D [44].

at $q=4/3$). Although an initial study on engineering feasibility has been done, further detailed study, particularly for the coil systems inside the VV as well as between the thermal shield and TF coils, must be carefully examined.

6) Construction of the integrated prediction codes

The modeling capability for integrating the core, pedestal, SOL and divertor regions has achieved remarkable progress [47-53]. For example, the evolution in ITER has been predicted by the LEHIGH -JETTO integrated modeling code [47], adopting mixed Bohm/gyro-Bohm anomalous core transport and the neoclassical pedestal transport and peeling and ballooning stability. The calculation results (Fig.14) show that the ITER baseline case yields Q=16.6 with the ion temperature at the top of the pedestal of 4.9keV. Other models [48, 49] based on ExB flow shear suppression of turbulence and peeling-ballooning

Fig.14: ITER base line scenario predicted by the LEHIGH -JETTO integrated modeling code [47],

stability reproduced experimental results. The TOPICS-IB code, with a stability code for the peeling-ballooning modes and a SOL model, found that the experimentally observed collisionality dependence of the ELM energy loss is caused by both the edge bootstrap current which changes the eigenfunction of the unstable modes and the parallel heat conduction in the SOL increasing with collisionality [50]. For further improvement of these simulations, the main remaining issues which need to be revsolved experimentally, and theoretically, are the dependence of pedestal width on plasma parameters and the evolution of the edge current during each ELM crash.

For accurate simulations, kinetic effects associated with long mean-free paths, finite gyroradius effects, and non-Maxwellian particles distributions become more important. Construction of such simulation codes are underway. TEMPEST is a gyrokinetic continuum code for edge physics studies where the particle distribution functions are represented as continuous functions on a configuration/velocity space mesh with full toroidal tokamak geometry [52]. A predictive gyrokinetic simulation of edge plasma by the XGC code [53] reveals that the turbulence suppression after the H-mode transition can be sustained by neoclassical sheared flow alone.
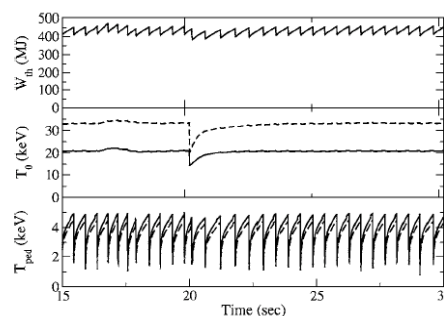
Reference

[1] ITPA , 'Progress in the ITER Physics Basis', Nucl. Fusion.
[2] V. Mukhovatov et al., Nucl. Fusion **43** (2003) 942.
[3] P.B. Snyder et al,, Plas Phys Contr Fusion **45** (2003) 1671
[4] H. Urano et al., Phys. Rev. Lett. 95 (2005) 035003.
[5] L.D. Horton et al., Nucl. Fusion **45** (2005) 856.
[6] M.F. Fenstaermacher, et al., Nucl. Fusion **45** (2005) 1493.
[7] D. Mossessian, et al., Phys. Plasmas, **10** (2003) 689.
[8] J.W. Hughes, et al., Phys. Plasmas, **13** (2006) 056103
[9] G. Saibene, et el., submitted to Nucl. Fusion
[10] H. Urano, et al., this conference , EX 5-1.
[11] V.Parail, et al., this conference,TH P8-5
[12] Y. Kamada et al., Plas Phys Contr Fusion **48** (2006) A419
[13] R.J. Groebner et al., Plas Phys Contr Fusion **48** (2006) A109.
[14] C. Maggi et al., this conference,
[15] S. Saarelma, et al, Plas Phys Contr Fusion **47** (2005) 713
[16] A.W. Leonard et al., Plas Phys Contr Fusion **48** (2006) A149.
[17] A. Kirk, et. al., Phys. Rev. Lett. **92** (2004) 245002.
[18] A. Kirk, et. al., Phys. Rev. Lett. **96** (2006) 185001.
[19] A. Loarte et al., Plas Phys Contr Fusion **45** (2003) 1549
[20] AUG
[21] K. Kamiya et al., Plas Phys Contr Fusion **48** (2006) A131.
[22] A. Loarte et al., Plas Phys Contr Fusion **44** (2002) 1815
[23] M. R. Wade et al., Phys. Plasmas **12** (2005) 056120.
[24] M. Yoshida et al., Plas Phys Contr Fusion **48** (2006) A209.
[25] H. R. Wilson et al., Plas Phys Contr Fusion **48** (2006) A71
[26] H.R. Wilson et al.,, Phys. Rev. Lett. **92** (2004) 175006-1

[27] G.T.A. Huysmans, Plas Phys Contr Fusion **EPS ISSUE** (2005)
[28] P.B. Snyder, et al.,Phys. Plasmas **12** (2005) 056115-1
[29] P.B. Snyder, et al, Phys Plasmas **9** (2002) 2037
[30] H.R. Wilson et al, This conference, TH/4-1Rb
[31] N. Oyama et al., Plas Phys Contr Fusion **48** (2006) A171.
[32] A.E. Hubbard et al., Plas Phys Contr Fusion **48** (2006) A121.
[33] W. Suttrop et al., Nucl. Fusion **45** (2005) 1399.
[34] J. Stober wt al., Nucl. Fusion **45** (2005) 1213.
[35] G. Saibene et al., Nucl. Fusion **45** (2005) 297.
[36] R. Maingi et al., Nucl. Fusion **45** (2005) 264.
[37] N. Oyama et al., Nucl. Fusion **45** (2005) 871.
[38] N. Oyama et al., submitted to Plas. Phys. Contr. Fusion
[39] P. Lang, et al., Nucl. Fusion **45** (2005) 502.
[40] A. Polevoi, et al., Plas Phys Contr Fusion **43** (2001) 1525.
[41] Sugihara, M., 10th ITPA PEP meeting, MIT (2006).
[42] A. Polevoi, et al., Nucl. Fusion **45** (2005) 1451.
[43] P. Lang, P., et al., Nucl. Fusion **44** (2004) 665.
[44] T.E. Evans et al., Phys. Rev. Lett. **92** (2004) 235003-1.
[45] T. E. Evans, et al., *Nature Physics* **2** (2006) 419-23.
[46] M. Becoulet , et al.,   this conference.
[47] T. Onjun et al., Phys. Plasmas 12 (2005) 082513
[48] J-S Lonnroth et al., Plas Phys Contr Fusion **46** (2004) 1197
[49] G. W. Pacher et al., Plas Phys Contr Fusion **46** (2004) A257.
[50] G. Bateman, et al., Plas Phys Contr Fusion **48** (2006) A93.
[51] N. Hayashi et al., this conference, TH 4-2
[52] X.Q. Xu, et al., this conference
[53] C.S. Chang et al., this conference